ACS NANO

www.acsnano.org

ARTICLE

Twisted Light-Induced Photocurrent in a Silicon Nanowire Field-Effect Transistor

Yi-Jie Feng, Kristan Bryan Simbulan, Tilo H. Yang, Ye-Ru Chen, Kai-Shin Li, Chia-Jung Chu, Ting-Hua Lu,* and Yann-Wen Lan*

Cite This: *ACS Nano* 2022, 16, 9297−9303

Read Online

ACCESS | Metrics & More | Article Recommendations | Supporting Information

ABSTRACT: **Light can possess orbital angular momentum (OAM), in addition to spin angular momentum (SAM), which offers nearly infinite possible values of momentum states, allowing a wider degree of freedom for information processing and communications. The OAM of light induces a selection rule that obeys the law of conservation of angular momentum as it interacts with a material, affecting the material's optical and electrical properties. In this work, silicon nanowire field-effect transistors are subjected to light with OAM, also known as twisted light. Electrical measurements on the devices consequently reveal photocurrent enhancements after incrementing the OAM of the incident light from 0ℏ (fundamental mode) to 5ℏ. Such a phenomenon is attributed to the enhancements of the photogating and the photoconductive effects under the influence of the OAM of light, the underlying mechanism of which is proposed and discussed using energy band diagrams. With these observations, a strategy for controlling photocurrent has been introduced, which can be a realization of the application in the field of optoelectronics technology.**

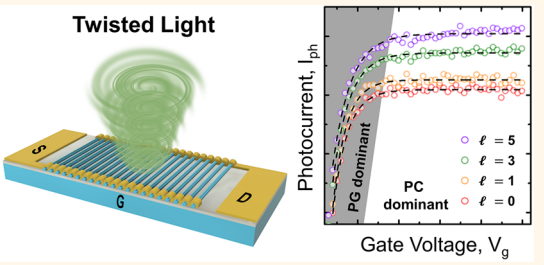

KEYWORDS: *twisted light, orbital angular momentum, silicon nanowires, photogain, photogating, photoconductive effects*

In terms of imaging and optical communication applications, a significant amount of attention has been focused on phototransistors—a critical component that detects and translates information carried by light into electrical output.[1,2] It is essential to gain deep insight into the phototransistor's effective light−matter interaction mechanisms to facilely control its photogenerated current. In principle, the intensity and wavelength of light can vary the photocurrent level in the photosensitive device. More interestingly, the spin angular momentum (SAM) of light can modulate the magnitude of the photocurrents, which is useful for spintronic devices and biochemical sensors, among others.[3−5] For instance, silicon nanowires interact with the SAM of light through a circular photogalvanic effect,[6] while some physical properties of metamaterials depend on the circular polarization of the incident light.[7−9]

Besides SAM, light can also possess a well-defined orbital angular momentum (OAM). Light with OAM and its interaction with materials have recently aroused the curiosity of many researchers. The OAM of the light−matter interaction has been gaining attention due to its potential applications that involve expanded data rates in optical communication, imaging improvements in astronomy, and developments in biology.[10,11] In addition, phenomena such as the spin−orbit interaction owing to the coupling of the SAM of light and the OAM of the surface plasmons,[12,13] a selection rule resulting from a successful transfer of the OAM of light into certain materials,[14−16] and charge accumulations due to the vortex motion of carriers[17] have emerged. Despite the OAM of light's promising features, its interaction with widely used materials has still not yet been explored. One of those materials is silicon nanowires (Si-NWs) which overcome the limitations, *e.g.*, narrow absorption range, of the bulk counterpart and exhibit fascinating optical properties that can be used in solar cells and biophotonics, to name a few.[18,19] The disadvantage of this one-dimensional nanostructure, however, is its low current gain.[20,21]

In this article, we have demonstrated the result of the interaction between OAM light and silicon nanowires. We have observed a noticeable photocurrent increase as we incremented the OAM of the incident light and attributed this to the impinging light with OAM, which enhances both the photoconductive- and the photogating-induced photocurrents. Lastly, the photocurrent's power dependence as a function of

Received: February 24, 2022
Accepted: June 14, 2022
Published: June 17, 2022

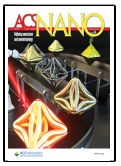

https://doi.org/10.1021/acsnano.2c01944
ACS Nano 2022, 16, 9297−9303

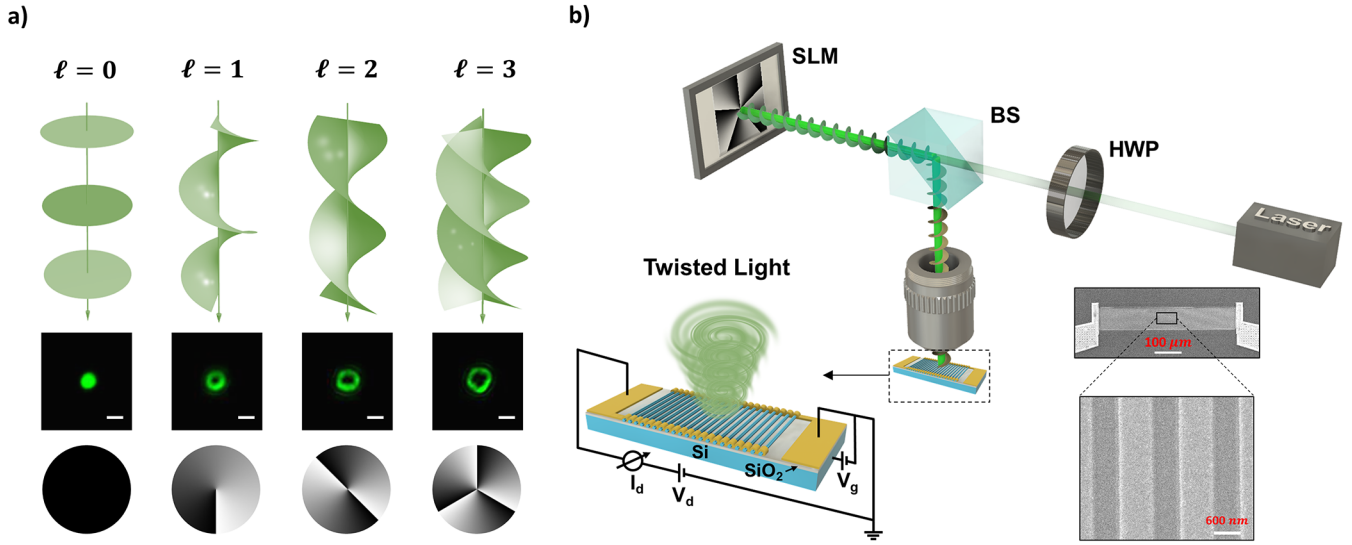

Figure 1. (a) Light with OAM is characterized by its helical wavefront; each of its photons possesses an OAM $L = l\hbar$. The second-row images reveal the actual beam spots indicated with a scale bar of 1 μm, while the third row shows the phase fronts, all corresponding to the indicated values of the light's l. (b) Schematic diagram of the Si-NWs' phototransistor, showing the parallel structure of the wires, the back gate voltage circuitry, and the normal incident twisted light. To generate the twisted light, an incident 532 nm fundamental-mode light (beam spot diameter of around 1 μm for $l = 0$) was illuminated onto a reflective spatial light modulator (SLM), which shapes the light depending on the phase pattern projected on the SLM interface, transforming the plane wave light ($l = 0$) into TL ($l \neq 0$). The terms BS and HWP refer to the beam splitter and half-wave plate, respectively. The SEM image of the Si-NWs, showing a width (W) of 600 nm and length (L) of 88 μm for each wire, is shown on the right-hand side of part b.

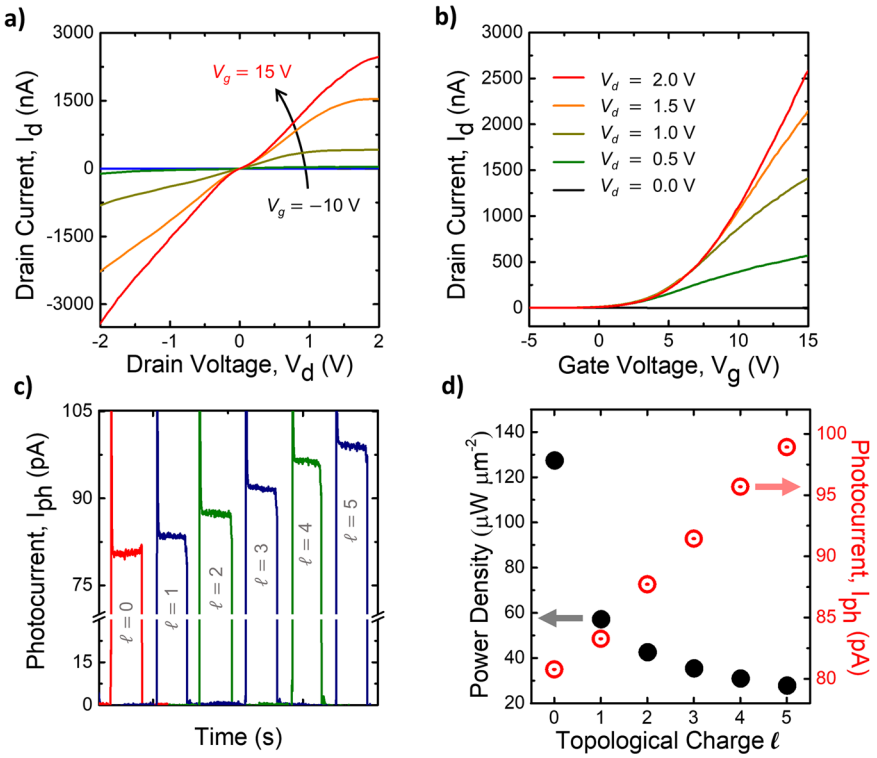

Figure 2. Typical electrical properties of the Si-NWs device. (a) I_d–V_d characteristics at V_g = −10 to 15 V, in 5 V intervals. (b) I_d–V_g characteristics at different V_d levels. (c) I_{ph}–T curves, revealing an increasing I_{ph} at incrementing OAM of light. The duration of the on-state is ∼20 s, while the off-state lasts for ∼10 s. (d) Incident power density and photocurrent (from part c) plotted against topological charge, showing that decreasing values of power density correspond to increasing photocurrent at incrementing OAM of light.

the OAM of light has been measured, indicating that the photocurrent gain exhibits a linear power dependence when illuminated with plane wave light and an increasing sublinear power dependence when used with light carrying OAM.

RESULTS AND DISCUSSION

The OAM of light manifests itself by way of an azimuthal phase term, $\exp(-il\phi)$, which causes its wave front to appear

https://doi.org/10.1021/acsnano.2c01944
ACS Nano 2022, 16, 9297−9303

in a helical shape; such a distinct structure has earned it the name twisted light (TL).[22] The wave front, optical microscope image, and phase distribution of the TL having different OAM values ($l\hbar$) per photon are altogether shown in Figure 1a. It is apparent that, at increasing integer values of its topological charge, l, the light manifests a more complicated wave front spatial distribution which can be verified by superimposing a spherical wave beam to a twisted light with distinct l to acquire interference patterns[23] as shown in Figure S1. Due to phase singularity, the beam center up to its proximity exhibits zero to very low intensity. Each of the TL's photons has an orbital angular momentum of $L = \pm l\hbar$, where l is called the topological charge and could have any integer value.[24,25] The recently attainable topological charge can be greater than 10,000.[26] Hence, due to a large number of available states, the interaction between TL and materials introduces an additional and wider degree of freedom.

The sensing material in this study is a back-gated field-effect transistor (FET) with about 500 Si-NWs connected in parallel. The optical setup and the SEM image are shown in Figure 1b. The channel length (L) and width (W) of a single wire are around 88 μm and 600 nm, respectively. Meanwhile, from the cross-sectional TEM image, as shown in Figure S2, the wire is confirmed as a single-crystal structure with a thickness of around 130 nm. The detailed information about the fabrication methods (Figure S3) is described in section III of the Supporting Information. An incident 532 nm light was illuminated onto a reflective spatial light modulator (SLM), which shapes the light depending on the phase pattern projected on the SLM interface. The SLM can transform a plane wave ($l = 0$) into a Laguerre−Gaussian beam or so-called TL ($l \neq 0$). The polarization of the incident OAM of light was perpendicular to the grating structure and was illuminated onto the material through a 50× objective lens with numerical aperture (NA) = 0.5. The comprehensive experiments were performed at room temperature and atmospheric pressure.

The device current in one of the fabricated transistors was initially measured in dark conditions to extract the pure electrical properties of the Si-NWs device, which shows an n-type characteristic as presented in its I_d−V_d and I_d−V_g curves in Figure 2a and b. In a general sense, a flow of free carriers can be initiated on a semiconducting material by striking it with photons of sufficient energy. The flow of photogenerated carriers, often called the photocurrent (I_{ph}), can be defined as[27]

$$I_{ph} = I_{illu} - I_{dark} \tag{1}$$

where I_{illu} and I_{dark} are the device current with and without illumination, respectively. If one intends to modulate the device photocurrent, two dominant mechanisms must be considered: the photoconductive (PC) and the photogating (PG) effects.[27−29] The PC effect defines a set of photocurrent that is accounted for by generated electron−hole (e-h) pairs due to the absorption of photons with energy near or greater than the band gap energy of the semiconducting material. Therein, any changes in the generated e-h pairs' density lead to extra carriers that enhance the conductivity and, thus, the photocurrent. The photocurrent produced via the PC effect (I_{ph}^{PC}) is independent of V_g and can be expressed as[27]

$$I_{ph}^{PC} = (W/L)V_{ds}\Delta\sigma \tag{2}$$

where $\Delta\sigma = q\mu\Delta n$ is the change in the material's conductivity, μ is the carrier mobility, and n is the carrier concentration.

The photocurrent produced via the PG effect (I_{ph}^{PG}), on the other hand, is associated with trap states that are formed on the surface or at the defect sites of the nanostructured material.[30] By illuminating the material, electrons/holes get trapped into the localized states, enabling the trapped carriers to function as a local gate that can further modulate the device current. The concentration of the trapped electrons/holes, and thus also I_{ph}^{PG}, is dependent on V_g. With the presence of trapped carriers acting like a local gate voltage, horizontal shifts in the material's I_d−V_g curve can be observed.[31] Accordingly, I_{ph}^{PG} can be described as[27]

$$I_{ph}^{PG} = g_m\Delta V_{TH} \tag{3}$$

where the transconductance $g_m = dI_d/dV_g$ and ΔV_{TH} is the threshold voltage shift relative to the dark conditions. Considering the above concepts, the following electrical measurements were performed while the device was impinged with incident light of varying OAM values.

A 532 nm incident light was primarily used to illuminate the Si-NWs device and was set to have a fixed sample power (100 μW) with variable OAM ($l\hbar$) values in all recorded measurements. The resulting I_{ph} versus time curves in Figure 2c reveal an enhancement of the photocurrent after increasing the OAM of light from $0\hbar$ to $5\hbar$. Considering the illuminated area from light carrying different topological charges, the power density and photocurrent (from Figure 2c) versus topological charge curves are presented in Figure 2d. Since lights with higher OAM values have larger beam spot sizes, their corresponding power densities are relatively lower. The above-mentioned trend is similarly observed even after considering only the illuminated parts of the Si-NWs structure. Notably, if the power density were solely responsible for the increases in current, the photocurrent should show the same trend as the power density of light. However, the photocurrent increases when a larger OAM of light is used. The effects of oblique incidences caused by the different l-dependent beam sizes through the objective lens in nanostructure gratings can also be excluded. This was determined after a control experiment was done wherein photocurrent measurements induced by fundamental-mode (without OAM) light having fixed power and increasing beam sizes resulted in decreasing photocurrents—a behavior that is opposite to our observations with the OAM of light. To further clarify the power-density-dependence issue on OAM-light-induced photocurrents and to minimize the influences of oblique incident light on the nanograting structure,[32] we, therefore, conducted the experiment of photocurrent enhancement by TL in an MoS_2-channeled device with nongrating structure as shown in Figure S4. The device is a continuous film of MoS_2 in which the channel width exceeds the beam spot. A strong light−matter interaction of MoS_2 manifests itself through a high photoresponse,[33] giving the same observation of higher photocurrent with respect to light with a larger OAM. The difference in the photocurrent levels between the $l = 5$ and $l = 0$ conditions may vary from sample to sample in both Si-NWs and MoS_2. However, all results conclude that higher photocurrents correspond to incident lights with larger OAM values. To investigate how the OAM of light enhances the photocurrent, the following transfer curves were subsequently measured.

https://doi.org/10.1021/acsnano.2c01944
ACS Nano 2022, 16, 9297−9303

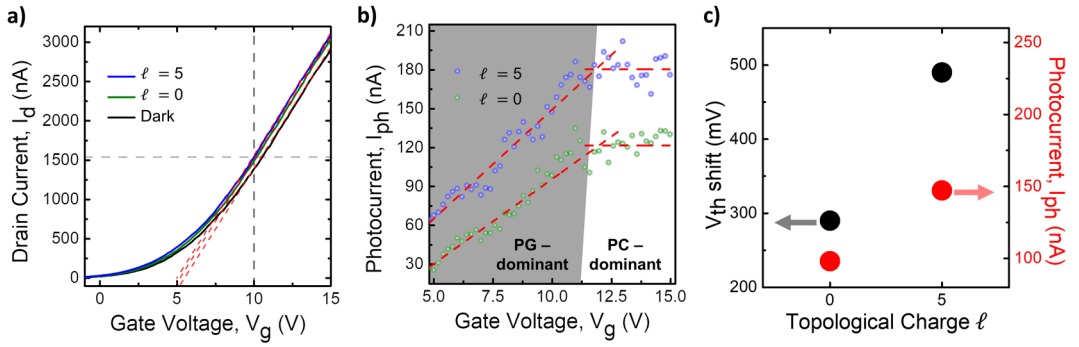

Figure 3. (a) Transfer curves at V_d = 2 V with a fixed optical power of 100 μW. (b) I_{ph}–V_g curves from part a, showing two regimes: the PG-dominant and PC-dominant regimes. (c) I_{ph} levels and V_{th} shifts plotted against the l of light. V_{th} is determined from part a by the extrapolation method, while I_{ph} is extracted from part b at V_g = 10 V.

Transfer curves were recorded with a fixed V_d = 2 V under dark and OAM-light-illuminated conditions as shown in Figure 3a. The red-dashed lines are the linear fits that determine the threshold voltages in each transfer curve using the extrapolation method. A shifting of the curves indicates the PG effect's involvement aside from the PC effect.[28] From the transfer curves, the transconductance can be extracted via a linear fitting method. The I_{ph}–V_g characteristics derived using eq 1 from Figure 3a are presented in Figure 3b to show two operating regimes: one that is strongly dependent on V_g and another that is independent. Deduced from the above-mentioned descriptions of the two effects, the V_g-dependent regime is dominated by the PG effect, and the V_g-independent one, by the PC effect. While the device is illuminated, increasing the positive value of the gate voltage to around V_g = 10 V fills up hole trap states, leading to a larger increase in current due to a dominant PG effect. At certain high values of V_g, however, the hole trap states get saturated, and the dominance switched in favor of the PC effect.

The enhancement of the photocurrent by TL can be credited to the improvements of both the PC and the PG effects. The heightening of the PC effect with l is apparent, especially when viewed at the PC-dominant regime, where the PG effect is expected to be very minimal. On the other hand, the involvement of the PG effect and its enhancements due to the OAM of light can be proved by extracting the ΔV_{TH} and I_{ph} at around V_g = 10 V, which is within the PG-dominant regime for both light conditions, as displayed in Figure 3c. In Figure 3c, ΔV_{TH} rises by around 200 mV from l = 0 to l = 5. ΔV_{TH} highly correlates with the corresponding OAM-of-light-induced photocurrent (see eq 3) at around V_g = 10 V in different light conditions. Besides, the rising of ΔV_{TH} also implies that a larger carrier concentration can be produced,[34,35] which indicates the presence and the strengthening of the effects via the OAM of light. To show the reproducibility of this experiment, another set of data with comparable results and with more detailed l are shown in Figure S5, which were measured from another device that bears a similar structure as the original one. Meanwhile, Figure S6 presents a similar trend of l-dependent photocurrent levels even after replacing the original objective lens with the ones having different magnifications and NA values. Herein, the objective lens with NA = 0.25 yielded lower enhancements.

In principle, the OAM of light has the potential to influence the absorption of incident photons in a material.[36] It has been reported that the OAM of light can enhance forbidden transitions in atoms[16,37,38] and, leaning on the preceding concept, can also vary the electron signal levels in semiconductors. These forbidden transition states in Si-NWs were predicted to have arisen from the quantized energy band of the nanowire.[39] More importantly, the specific unlocked transition is determined via the conservation of angular momentum, which also causes a conelike transition from a single state under its valence band to superposition states in the conduction band.[40] With more transition paths, a better absorption of light can be achieved, and as a result, enhancements of the I_{ph}^{PC} can be observed. Moreover, with a better absorption of photons, the probability of getting more carriers in trap states is also increased by the TL, therefore increasing I_{ph}^{PG} as well. The potential mechanism for the enhancements in both I_{ph}^{PC} and I_{ph}^{PG} is proposed and illustrated through band diagrams as shown in Figure 4. Under the equilibrium (dark) state and high enough applied gate voltages, the Fermi level is near the conduction band (Figure 4a), which is due to the n-type characteristic. Considering the PC effect, the illumination of light in the material will cause an increase in the conduction band carrier concentration resulting in an increase in current (Figure 4b). Notably, there are some forbidden transitions in the case of fundamental light (l = 0), which does not contribute to the current. In the presence of trapped states, however, the PG effect also comes into play (Figure 4c). Since the Fermi level is initially closer to the conduction band, a part of the electrons has already been filled in the trapped states. Therefore, the rate of increase of the density of photoinduced trapped holes is far greater than that of the photoinduced trapped electrons, thereby enhancing the photocurrent via the photogating effect.[41] Accordingly, if the Fermi level is originally not close to the conduction band, a negative photoresponse can be observed.[41] The two effects are schematically exemplified in Figure 4d. Phenomenologically, because of the increased carrier concentration through the possible enhanced forbidden transitions,[40] TL can improve the I_{ph}^{PC}. Plus, we further argue that TL can induce more carriers that can fill in the trapped states, increasing the I_{ph}^{PG}, as directly evidenced by the following power-dependent result.

The photocurrent versus laser power (I_{ph}–P_{opt}) curve, focused on either the PG-dominant regime (V_g = 10 V) or the PC-dominant regime (V_g = 15 V), as a function of the OAM of light is studied and presented in Figure 5. In Figure 5a, the power factor (α) is extracted from the linear fitting result of the logarithmic-scaled I_{ph}–P_{opt} curves. The complete set of the I_{ph}–P_{opt} data, including V_g = 10 V and V_g = 15 V, are attached in Figure S7, and the corresponding raw data of the I_{ph}–V_g curve are provided in Figure S8. As shown in the inset

https://doi.org/10.1021/acsnano.2c01944
ACS Nano 2022, 16, 9297–9303

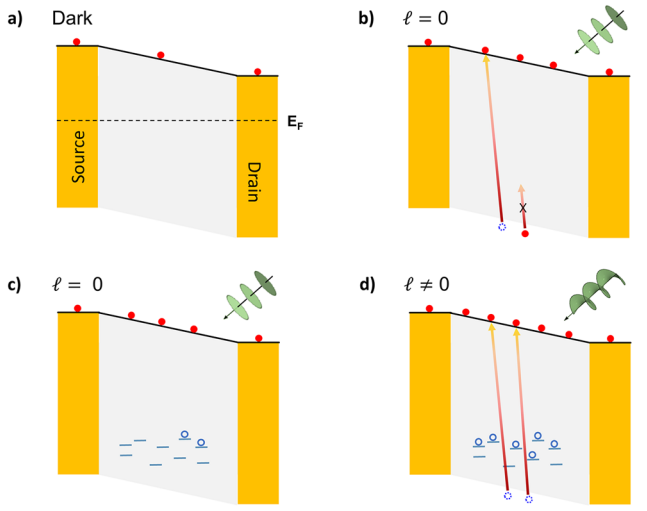

Figure 4. Schematic of the photoconductive (PC) and photogating (PG) effects at different light conditions. (a) Band alignment for the Si-NWs device under a fixed bias voltage without illumination. The Fermi level is close to the conduction band because of the material's n-type characteristic. (b) In the case of an incident fundamental light ($l = 0$), the PC effect contributes photogenerated carriers to the conduction band, leading to a higher photocurrent. Note that some of the transitions are not allowed for the case of fundamental light. (c) With an incident fundamental light ($l = 0$), light induces photogenerated electrons and holes in the material. Considering the trapped states, holes get trapped into these localized states, which act as a local gate that modulates the device current (*i.e.* PG effect). (d) Under the illumination of light with OAM, some forbidden transition channels are allowed to enhance the absorption of light, thereby enhancing the carrier concentration in the conduction band as well as the density of trapped holes in trapped states.

of Figure 5a, the α is constantly decreasing from 0.97 to 0.76 as the l of light varies from 0 to 5 at V_g = 10 V. Note that the α is further decreased at V_g = 15 V. It is instructive to determine the generated excess carriers for understanding the photocurrent's sublinear behavior relative to the optical power. The total number of photons arriving at the surface of the material is $P_{opt}/h\nu$ per unit time. Given the device height D, the generation rate of carriers per unit volume (G_e) is expressed as[42]

$$G_e = \frac{n}{\tau} = \frac{\eta(P_{opt}/h\nu)}{WLD} \tag{4}$$

where, P_{opt} is the optical power, n is the excess carrier density, η is the quantum efficiency, and τ is the carrier lifetime. Based on eqs 2 and 4, the incident optical power proportionally affects the photocurrent *via* the PC effect, *i.e.*, $I_{ph} \propto P_{opt}^{\alpha}$, where the power factor α should be 1.[43] However, the decreasing values of the power factor indicate that, besides the PC effect, other effects contribute significantly. The effect from the power densities of light possessing different OAM values[44] is excluded as shown in section IX of the Supporting Information. In this regard, as the OAM of the incident light progressively increases, the PG effect becomes more and more considerable. Therefore, the strengths of the PG and PC effects at a specific gate voltage can be determined via the power factor, and the lower the power factor is, the less dominant is the PC effect involved. This sublinear behavior in the power-dependent photocurrent measurement can be another evidence of the PG effect's involvement in the reported result.[31,45] On top of that, from a different perspective, Figure 5b, showing the relationship of the photocurrent levels and the l of the exciting light at selected values of the optical power, implies a possible extra degree of freedom induced by TL.

CONCLUSIONS

A progressively increasing photocurrent as the OAM of the incident light increases was recorded in this work. Two photocurrent regimes were revealed: the photoconductive and the photogating effects, in which dominance depends on the applied V_g. Accordingly, the OAM of light improves the photocurrent in both regimes. It has been inferred that the increase in the PC-induced currents is caused by the enhanced forbidden transitions brought by the inherent OAM of light, which can improve the absorption of photons in the material, leading to an increase in the density of photoinduced carriers. Consequently, improvements of the PG-induced currents are triggered by the resulting increase of the density of photoinduced trapped holes. Such is supported by the results of the power-dependent measurements, which reveal a sublinear relation with an incident OAM light, compared to a linear-dependent behavior with plane wave light, proving the heightening of the PG effect under the influence of the OAM of light. Through this work, we introduce a way to increase the

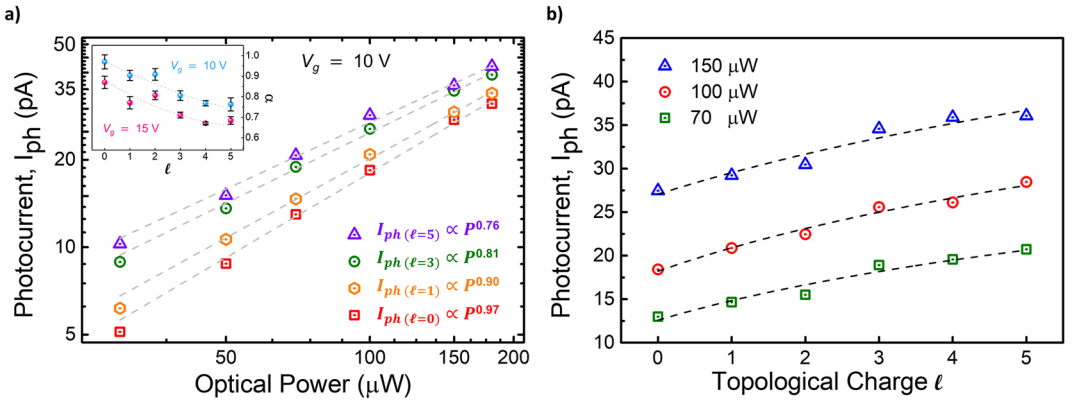

Figure 5. Power-dependent photocurrent at fixed V_g = 10 V and V_{ds} = 1 V. (a) I_{ph}–*Power* curves in log scale as a function of the OAM of light. The power factor (α) decreases as the value of the OAM of light ($\sim l$) increases, as explicitly displayed in the inset, wherein the dashed lines are guides to the eye. (b) $I_{ph} - l$ plots at selected optical power levels.

https://doi.org/10.1021/acsnano.2c01944
ACS Nano 2022, 16, 9297−9303

photogain, which can potentially improve the performance of Si-NWs photodetectors. Since light can possess near-infinite OAM states, other materials or device structures can be engineered to take advantage of the particular property of twisted light. Our results may call for further investigations of the OAM light−matter interaction by using first-principles theory to unravel the physics behind this observed phenomenon. Based on that, this additional degree of freedom for optoelectronics might be extensively explored toward practical applications.

METHODS

Electrical Measurements. All experiments presented in this paper were performed at room temperature and atmospheric pressure. A 50× long-working-distance objective lens (NA = 0.5) was used to focus the laser. The solid-state laser generates plane wave light with a wavelength of 532 nm. The conversion of it to twisted light was done by HOLOEYE's spatial light modulator system (PLUTO-2), which was based on a reflective liquid crystal microdisplay with 1920 × 1080 pixel resolution and 8.0 μm pixel pitch. Twisted light was then perpendicularly illuminated onto the device for electrical measurements. For electrical characterization, the device was mounted on the probe station while three-terminal electrical measurements were performed via the semiconductor analyzer (Keithley 2636B).

Optical Power Measurement. The optical power was measured using Compact Power and Energy Meter Console − PM100D with Standard Photodiode Power Sensors − S121C from THORLABS. The optical power of each light source was measured after the objective lens, *i.e.*, after the SLM. The whole process of power measurement is as follows: before the Si-NWs device was placed, the sensor was installed first under the objective lens at the exact height and position where the Si-NWs device would be set. Because the power meter was set to the same position as the Si-NWs device, it was called the "sample power". As seen from the information on Standard Photodiode Power Sensors − S121C, the active detector area is 9.7 mm × 9.7 mm, which is much larger than the beam spot that we used; moreover, instead of power density, this detector measures power, because within a certain range, changing the perpendicular distance (thus, also changing the beam spot size) of the detector from the lens does not vary the power level that it detects.

ASSOCIATED CONTENT

Supporting Information

The Supporting Information is available free of charge at https://pubs.acs.org/doi/10.1021/acsnano.2c01944.

Helical wave front of light possessing the indicated l; TEM image of the Si-NW; device fabrication; photocurrent enhancement in a single-channeled MoS_2 device; I_d−V_g characteristic curves under illumination of light with different OAM conditions; I_d−V_g characteristic curves under illumination of light with different OAM conditions when using different objective lens; complete data of the power-dependent photocurrent under illumination of light with different OAM conditions; raw data of I_{ph}−V_g under illumination of light with different optical power and OAM conditions; and normalized intensity distribution of light possessing each l (PDF)

AUTHOR INFORMATION

Corresponding Authors

Ting-Hua Lu − *Department of Physics, National Taiwan Normal University, Taipei 11677, Taiwan*

Yann-Wen Lan − *Department of Physics, National Taiwan Normal University, Taipei 11677, Taiwan;* orcid.org/0000-0003-2403-1357

Authors

Yi-Jie Feng − *Department of Physics, National Taiwan Normal University, Taipei 11677, Taiwan*

Kristan Bryan Simbulan − *Department of Physics, National Taiwan Normal University, Taipei 11677, Taiwan; Department of Mathematics and Physics, University of Santo Tomas, Manila 1008, Philippines;* orcid.org/0000-0001-9102-5876

Tilo H. Yang − *Department of Physics, National Taiwan Normal University, Taipei 11677, Taiwan*

Ye-Ru Chen − *Department of Physics, National Taiwan Normal University, Taipei 11677, Taiwan*

Kai-Shin Li − *Taiwan Semiconductor Research Institute, National Applied Research Laboratories, Hsinchu 30078, Taiwan*

Chia-Jung Chu − *Silicon Based Molecular Sensoring Technology CO., Ltd. (Molsentech), Taipei 11571, Taiwan*

Complete contact information is available at: https://pubs.acs.org/10.1021/acsnano.2c01944

Author Contributions

Y.J.F. performed the experiments/measurements, data analysis, and calculations. Y.J.F. and K.B.S. did the paper survey and built the mechanism. T. H.Y. took the SEM image and illustrated the schematic diagram. Y.J.F., K.B.S., T.H.Y., and Y.W.L. completed this paper. Y.R.C. collected data from MoS_2. K.S.L. performed the experiment of TEM. C.J.C. provided the Si-NWs sample. Y.W.L. and T.H.L. supervised this research. All authors have read and approved the manuscript. All authors discussed the results and commented on the manuscript.

Notes

The authors declare no competing financial interest.

ACKNOWLEDGMENTS

This work was supported by the National Science Council, Taiwan, under contract Nos. MOST 108-2112-M-003-010-MY3, MOST 108-2112-M-003-009, and MOST-111-2119-M-008-003-MBK.

REFERENCES

(1) Liu, C.; Guo, J.; Yu, L.; Li, J.; Zhang, M.; Li, H.; Shi, Y.; Dai, D. Silicon/2d-Material Photodetectors: From near-Infrared to Mid-Infrared. *Light Sci. Appl.* **2021**, *10*, 123.

(2) Zhuge, F.; Zheng, Z.; Luo, P.; Lv, L.; Huang, Y.; Li, H.; Zhai, T. Nanostructured Materials and Architectures for Advanced Infrared Photodetection. *Advanced Materials Technologies* **2017**, *2*, 1700005.

(3) Eginligil, M.; Cao, B.; Wang, Z.; Shen, X.; Cong, C.; Shang, J.; Soci, C.; Yu, T. Dichroic Spin-Valley Photocurrent in Monolayer Molybdenum Disulphide. *Nat. Commun.* **2015**, *6*, 7636.

(4) Mak, K. F.; He, K.; Shan, J.; Heinz, T. F. Control of Valley Polarization in Monolayer Mos2 by Optical Helicity. *Nat. Nanotechnol* **2012**, *7*, 494−498.

(5) Saushin, A. S.; Mikheev, K. G.; Styapshin, V. M.; Mikheev, G. M. Direct Measurement of the Circular Photocurrent in the Ag/Pd Nanocomposites. *Journal of Nanophotonics* **2017**, *11*, 032508.

(6) Dhara, S.; Mele, E. J.; Agarwal, R. Voltage-Tunable Circular Photogalvanic Effect in Silicon Nanowires. *Science* **2015**, *349*, 726−729.

(7) Yao, K.; Liu, Y. Enhancing Circular Dichroism by Chiral Hotspots in Silicon Nanocube Dimers. *Nanoscale* **2018**, *10*, 8779−8786.
(8) Gandolfi, M.; Tognazzi, A.; Rocco, D.; De Angelis, C.; Carletti, L. Near-Unity Third-Harmonic Circular Dichroism Driven by a Quasibound State in the Continuum in Asymmetric Silicon Metasurfaces. *Phys. Rev. A* **2021**, *104*, DOI: 10.1103/PhysRevA.104.023524.
(9) Proscia, N. V.; Moocarme, M.; Chang, R.; Kretzschmar, I.; Menon, V. M.; Vuong, L. T. Control of Photo-Induced Voltages in Plasmonic Crystals Via Spin-Orbit Interactions. *Opt. Express* **2016**, *24*, 10402−10411.
(10) Swartzlander, G. A., Jr. The Optical Vortex Lens. *Opt. Photon. News* **2006**, *17*, 39−43.
(11) Molina-Terriza, G.; Torres, J. P.; Torner, L. Twisted Photons. *Nat. Phys.* **2007**, *3*, 305−310.
(12) Garoli, D.; Zilio, P.; De Angelis, F.; Gorodetski, Y. Helicity Locking of Chiral Light Emitted from a Plasmonic Nanotaper. *Nanoscale* **2017**, *9*, 6965−6969.
(13) Gorodetski, Y.; Shitrit, N.; Bretner, I.; Kleiner, V.; Hasman, E. Observation of Optical Spin Symmetry Breaking in Nanoapertures. *Nano Lett.* **2009**, *9*, 3016−3019.
(14) Simbulan, K. B.; Huang, T. D.; Peng, G. H.; Li, F.; Gomez Sanchez, O. J.; Lin, J. D.; Lu, C. I.; Yang, C. S.; Qi, J.; Cheng, S. J.; Lu, T. H.; Lan, Y. W. Selective Photoexcitation of Finite-Momentum Excitons in Monolayer Mos2 by Twisted Light. *ACS Nano* **2021**, *15*, 3481−3489.
(15) Sordillo, L. A.; Mamani, S.; Sharonov, M.; Alfano, R. R. The Interaction of Twisted Laguerre-Gaussian Light with a Gaas Photocathode to Investigate Photogenerated Polarized Electrons. *Appl. Phys. Lett.* **2019**, *114*, 041104.
(16) Clayburn, N. B.; McCarter, J. L.; Dreiling, J. M.; Poelker, M.; Ryan, D. M.; Gay, T. J. Search for Spin-Polarized Photoemission from Gas Using Light with Orbital Angular Momentum. *Phys. Rev. B* **2013**, *87*, DOI: 10.1103/PhysRevB.87.035204.
(17) Watzel, J.; Berakdar, J. Centrifugal Photovoltaic and Photogalvanic Effects Driven by Structured Light. *Sci. Rep* **2016**, *6*, 21475.
(18) Tsakalakos, L.; Balch, J.; Fronheiser, J.; Korevaar, B. A.; Sulima, O.; Rand, J. Silicon Nanowire Solar Cells. *Appl. Phys. Lett.* **2007**, *91*, 233117.
(19) Zhang, G.-J.; Zhang, L.; Huang, M. J.; Luo, Z. H. H.; Tay, G. K. I.; Lim, E.-J. A.; Kang, T. G.; Chen, Y. Silicon Nanowire Biosensor for Highly Sensitive and Rapid Detection of Dengue Virus. *Sens. Actuators, B* **2010**, *146*, 138−144.
(20) Xu, T.; Lambert, Y.; Krzeminski, C.; Grandidier, B.; Stiévenard, D.; Lévêque, G.; Akjouj, A.; Pennec, Y.; Djafari-Rouhani, B. Optical Absorption of Silicon Nanowires. *J. Appl. Phys.* **2012**, *112*, 033506.
(21) Xu, Q.; Dan, Y. Uncovering the Density of Nanowire Surface Trap States Hidden in the Transient Photoconductance. *Nanoscale* **2016**, *8*, 15934−15938.
(22) Padgett, M.; Courtial, J.; Allen, L. Light's Orbital Angular Momentum. *Phys. Today* **2004**, *57*, 35−40.
(23) Carpentier, A. V.; Michinel, H.; Salgueiro, J. R.; Olivieri, D. Making Optical Vortices with Computer-Generated Holograms. *American Journal of Physics* **2008**, *76*, 916−921.
(24) Shen, Y.; Wang, X.; Xie, Z.; Min, C.; Fu, X.; Liu, Q.; Gong, M.; Yuan, X. Optical Vortices 30 Years On: Oam Manipulation from Topological Charge to Multiple Singularities. *Light Sci. Appl.* **2019**, *8*, 90.
(25) Allen, L.; Beijersbergen, M. W.; Spreeuw, R. J.; Woerdman, J. P. Orbital Angular Momentum of Light and the Transformation of Laguerre-Gaussian Laser Modes. *Phys. Rev. A* **1992**, *45*, 8185−8189.
(26) Fickler, R.; Campbell, G.; Buchler, B.; Lam, P. K.; Zeilinger, A. Quantum Entanglement of Angular Momentum States with Quantum Numbers up to 10,010. *Proc. Natl. Acad. Sci. U. S. A.* **2016**, *113*, 13642−13647.
(27) Furchi, M. M.; Polyushkin, D. K.; Pospischil, A.; Mueller, T. Mechanisms of Photoconductivity in Atomically Thin Mos2. *Nano Lett.* **2014**, *14*, 6165−6170.
(28) Buscema, M.; Island, J. O.; Groenendijk, D. J.; Blanter, S. I.; Steele, G. A.; van der Zant, H. S.; Castellanos-Gomez, A. Photocurrent Generation with Two-Dimensional Van Der Waals Semiconductors. *Chem. Soc. Rev.* **2015**, *44*, 3691−3718.
(29) Di Bartolomeo, A.; Genovese, L.; Foller, T.; Giubileo, F.; Luongo, G.; Croin, L.; Liang, S. J.; Ang, L. K.; Schleberger, M. Electrical Transport and Persistent Photoconductivity in Monolayer Mos2 Phototransistors. *Nanotechnology* **2017**, *28*, 214002.
(30) Wolkin, M. V.; Jorne, J.; Fauchet, P. M.; Allan, G.; Delerue, C. Electronic States and Luminescence in Porous Silicon Quantum Dots: The Role of Oxygen. *Phys. Rev. Lett.* **1999**, *82*, 197−200.
(31) Island, J. O.; Blanter, S. I.; Buscema, M.; van der Zant, H. S.; Castellanos-Gomez, A. Gate Controlled Photocurrent Generation Mechanisms in High-Gain in(2)Se(3) Phototransistors. *Nano Lett.* **2015**, *15*, 7853−7858.
(32) Darweesh, A. A.; Bauman, S. J.; Debu, D. T.; Herzog, J. B. The Role of Rayleigh-Wood Anomalies and Surface Plasmons in Optical Enhancement for Nano-Gratings. *Nanomaterials (Basel)* **2018**, *8*, 809.
(33) Zhang, W.; Huang, J. K.; Chen, C. H.; Chang, Y. H.; Cheng, Y. J.; Li, L. J. High-Gain Phototransistors Based on a Cvd Mos(2) Monolayer. *Adv. Mater.* **2013**, *25*, 3456−3461.
(34) Lee, J.-K.; Sung, H.; Jang, M. S.; Yoon, H.; Choi, M. Reliable Doping and Carrier Concentration Control in Graphene by Aerosol-Derived Metal Nanoparticles. *Journal of Materials Chemistry C* **2015**, *3*, 8294−8299.
(35) Nguyen, L.-N.; Chang, W.-H.; Chen, C.-D.; Lan, Y.-W. Superior Phototransistors Based on a Single Zno Nanoparticle with High Mobility and Ultrafast Response Time. *Nanoscale Horizons* **2020**, *5*, 82−88.
(36) Simbulan, K. B.; Feng, Y. J.; Chang, W. H.; Lu, C. I.; Lu, T. H.; Lan, Y. W. Twisted Light-Enhanced Photovoltaic Effect. *ACS Nano* **2021**, *15*, 14822−14829.
(37) Schmiegelow, C. T.; Schulz, J.; Kaufmann, H.; Ruster, T.; Poschinger, U. G.; Schmidt-Kaler, F. Transfer of Optical Orbital Angular Momentum to a Bound Electron. *Nat. Commun.* **2016**, *7*, 12998.
(38) Babiker, M.; Andrews, D. L.; Lembessis, V. E. Atoms in Complex Twisted Light. *Journal of Optics* **2019**, *21*, 013001.
(39) Zhang, L.; Luo, J.-W.; Franceschetti, A.; Zunger, A. Excitons and Excitonic Fine Structures in Si Nanowires: Prediction of an Electronic State Crossover with Diameter Changes. *Phys. Rev. B* **2011**, *84*, 075404.
(40) Quinteiro, G. F.; Tamborenea, P. I. Theory of the Optical Absorption of Light Carrying Orbital Angular Momentum by Semiconductors. *EPL (Europhysics Letters)* **2009**, *85*, 47001.
(41) Lee, I.; Kang, W. T.; Kim, J. E.; Kim, Y. R.; Won, U. Y.; Lee, Y. H.; Yu, W. J. Photoinduced Tuning of Schottky Barrier Height in Graphene/Mos2 Heterojunction for Ultrahigh Performance Short Channel Phototransistor. *ACS Nano* **2020**, *14*, 7574−7580.
(42) Sze, S. M.; Ng, K. K. *Physics of Semiconductor Devices*; Wiley, 2006.
(43) Yin, Z.; Li, H.; Li, H.; Jiang, L.; Shi, Y.; Sun, Y.; Lu, G.; Zhang, Q.; Chen, X.; Zhang, H. Single-Layer Mos2 Phototransistors. *ACS Nano* **2012**, *6*, 74−80.
(44) Longman, A.; Fedosejevs, R. Optimal Laguerre-Gaussian Modes for High-Intensity Optical Vortices. *J. Opt Soc. Am. A Opt Image Sci. Vis* **2020**, *37*, 841−848.
(45) Wu, J. Y.; Chun, Y. T.; Li, S.; Zhang, T.; Wang, J.; Shrestha, P. K.; Chu, D. Broadband MoS_2 Field-Effect Phototransistors: Ultrasensitive Visible-Light Photoresponse and Negative Infrared Photoresponse. *Adv. Mater.* **2018**, *30*, 1705880.

https://doi.org/10.1021/acsnano.2c01944
ACS Nano 2022, 16, 9297−9303